Published in final edited form as:
J Magn Reson Imaging. 2011 September ; 34(3): 662–669. doi:10.1002/jmri.22694.

In Situ Active Control of Noise in a 4-Tesla MRI Scanner

Mingfeng Li, Ph.D.[1], **Brent Rudd, Ph.D.**[1], **Teik C. Lim, Ph.D.**[1], and **Jing-Huei Lee, Ph.D.**[2,3,*]

[1] School of Dynamic Systems, Mechanical Engineering, P.O. Box 210072, University of Cincinnati, Cincinnati, OH 45221

[2] School of Energy, Environmental, Biological and Medical Engineering, P.O. Box 670048, University of Cincinnati, Cincinnati, OH 45221

[3] Center for Imaging Research, P.O. Box 670583, University of Cincinnati, Cincinnati, OH 45267

Abstract

Purpose—To evaluate the effectiveness of the proposed active noise control (ANC) system for the reduction of the acoustic noise emission generated by a 4 T MRI scanner during operation and to assess the feasibility of developing an ANC device that can be deployed *in situ*.

Materials and Methods—Three typical scanning sequences, namely EPI (echo planar imaging), GEMS (gradient echo multi-slice) and MDEFT (Modified Driven Equilibrium Fourier Transform), were used for evaluating the performance of the ANC system, which was composed of a magnetic compatible headset and a multiple reference feedforward filtered-x least mean square controller.

Results—The greatest reduction, about 55 dB, was achieved at the harmonic at a frequency of 1.3 kHz in the GEMS case. Approximately 21 dB and 30 dBA overall reduction was achieved for GEMS noise across the entire audible frequency range. For the MDEFT sequence, the control system achieved 14 dB and 14 dBA overall reduction in the audible frequency range, while 13 dB and 14 dBA reduction was obtained for the EPI case.

Conclusion—The result is highly encouraging because it shows great potential for treating MRI noise with an ANC application during real time scanning.

Keywords

MRI acoustics; noise; sound; active noise control

INTRODUCTION

Although MRI has evolved into an important imaging tool in medical diagnosis and research, the noise emitted by the scanner during operation remains a concern because it interferes with communication and could be hazardous to hearing. It is well known that the MRI acoustic noise generated during imaging is very loud. In 1989, Hurwitz et. al. (1) measured the sound pressure level (SPL) at the magnet isocenter and reported levels between 82 and 93 dBA for static magnetic field strengths of 0.35 to 1.5 T. In a study by Ravicz et. al. (2), the measured SPLs of two scanners (1.5 and 3 T) operated with EPI sequences were found to vary from 123 to 138 dB. In our study (3), SPLs as high as 130 dB were recorded from a 4 T MRI machine running an EPI sequence. It is generally agreed that SPLs are greater at higher magnetic fields. Safety issues related to the use of MRI such as

[*]Corresponding Author / Reprint Info: Jing-Huei Lee, Ph.D., Center for Imaging Research, Suite E685 MSB, P.O. Box 670583, University of Cincinnati, Cincinnati, OH 45267, Tel: 513-558-5676 Fax: 513-558-7164 jing-huei.lee@uc.edu.

the physiological effects of loud noise, radio frequency (RF) exposure, and the magnetic field environment, have been documented (4). Numerous previous studies have shown that exposure to high levels of MRI sound could cause psychological problems including temporary hearing threshold shifts, anxiety, stress, annoyance, mental fatigue and fear (5–8). Hence, it is strongly suggested and commonly required that all patients and healthcare workers in or near the scanner chamber wear ear protection (9–11).

It is well known that the acoustic noise emitted during MRI scanning is a result of the rapidly switching electric currents that drive the pulse gradient magnetic fields. The Lorentz forces caused by the electrical current applied to the gradient coils in the main static field excite the structural components of the MRI scanner. The structural excitation effectively turns the MRI system into a loudspeaker (12–13). The magnitude of structural vibration that causes the acoustic radiation is dependent on magnetic field strength, gradient strength, scanner structure and geometry, spatial settings, and the frequency and waveform of the switching current (13–14).

Several remedies have been proposed to treat MRI sound emissions (14). Designing “silent” MRI pulse sequences is one option to reduce the MRI generated noise (15). However, this approach may limit the imaging applications for some cases. A traditional way to deal with the high levels of MRI noise is to use a passive control approach. The high level noise is reduced by using absorbing materials or modifying the system dynamics to dissipate or redistribute acoustic emissions. A common mode of implementation is having the patient wear ear plugs and/or a headset. This approach usually works well for high frequency noise stimuli but is less effective at lower frequencies. To increase the efficiency of earmuff/headset noise reduction in the low frequency range, the device would need to be bulky, which is not practical for the MRI application due to the limited space inside the RF head coil. In addition, the patient’s comfort will be impacted by wearing a large earmuff/headset. Alternatively, active noise control (ANC), which introduces an out-of-phase secondary acoustic wave form to cancel the sound source response, is a more effective approach for controlling low frequency noise and might allow for a reduction in the weight of headsets. This is desirable for patient’s comfort, particularly during long scans.

In recent years, using active control for MRI noise reduction has received attention from many researchers (16–27). To apply the ANC technique to MRI noise suppression, two issues need to be addressed. First, one needs to identify an appropriate actuation approach. Because of the unique magnetic environment, an MRI compatible speaker is required to deliver the control acoustic wave to the desired space. Second, an optimal controller must be developed for effectively reducing the sound pressure level (SPL). The earliest application of ANC on MRI noise was conducted by Goldman et al. (16). They implemented an MRI ANC system by injecting a synthesized anti-phase signal, which is generated by inverting the phase of the dominant frequency components of a recorded MRI signal. However, this method lacks flexibility in tracking changes of system properties and MRI response signals. Furthermore, in their system, a pneumatic tube is used to deliver the anti-phase sound, which introduces an additional time delay to the system and consequently degrades performance. Mechefske and Geris (20) investigated two ANC systems; a headset-based system and a pneumatic tube-based system. The former was equipped with non-magnetic components (speakers, microphones, and preamps) inside an ear defender, while the latter used a tube to transmit noise cancellation signals to the headset. Their results revealed that the tube-based system was less effective than the headset-based system due to the time delay created by the length of tube used.

In 1995, Pla et al. (17) used a pair of piezoelectric speakers placed close to the subject’s ears and an adaptive controller with a multi-channel filtered-x least mean squares (FXLMS)

algorithm as the ANC system. Up to 25 dB of noise reduction at frequencies up to 1.2 kHz was reported for their application. However, the MRI noises treated were primarily the first few harmonics. Furthermore, due to limited performance with this arrangement, patients will still be required to wear an earmuff.

Later, McJury et al. (18) and Chen et al. (19) tested their own system (McJury used a feedforward controller including a filtered-U LMS (FULMS) algorithm and Chen proposed a feedback controller system with a cascading neural-network architecture) in the laboratory (i.e. a non *in situ* study) using pre-recorded MRI scanner noise played through a loudspeaker. However, their system performances were all limited.

More recently, Kahana et al. (21) implemented a feedforward ANC system in an MRI communication system by utilizing an optoacoustic based (i.e. a piezoelectric speaker driven by optical signals) ear defender. Their results showed 35–50 dB attenuation at the fundamental frequency component. This value was in addition to 15 dB of passive attenuation realized by the slim ear defender headset. Furthermore, Chambers and his colleagues implemented an ANC system on an electrostatic headphone for MRI noise and evaluated the system performance using acoustic, psychophysical and neuroimaging measurements (22–24). In the most intense component of the scanner noises, an objective reduction of 30–40 dB was obtained for the frequency between 0.5 kHz and 3.5 kHz.

In 2008, we used hybrid control which combined a simple feedforward controller and an H-infinity feedback controller to treat the MRI acoustic response, generated by an Echo Planar Imaging (EPI) sequence, which is dominated by a principal harmonic and its sideband (25). Later, a feedforward system with multiple reference signals was proposed for various common scanning sequences including gradient echo multi-slice (GEMS) (26) and EPI (27). Significant reduction was obtained during both physical simulation and *in situ* tests (26–27). However, the reduction observed during in situ tests was limited to frequencies up to 2 kHz which is the effective bandwidth of the speaker system. The physical simulation tests have performed well to slightly higher frequencies, albeit in a more controlled environment.

In this study, the ANC system was enhanced with the goal of achieving improved performance at higher frequencies by tuning the reference signal over different frequency ranges. Furthermore, multiple reference signals including both gradient excitation and microphone signals are used in the proposed system. It was tested during live imaging scans on a 4 T scanner. Three different scanning sequences were tested: EPI, GEMS and MDEFT. The results showed that the effective frequency range of the ANC system has been increased to 5 kHz which covers most dominant frequency components of typical MRI scanner noise.

MATERIALS AND METHODS

Experimental Setup

A 4 T Varian Unity INOVA whole-body MRI scanner (Palo Alto, CA) was used to obtain all test results presented here. The acoustic noise measurements were made in the vicinity of the scanner bore isocenter where the patient's head is normally located during scanning. A humanoid dummy (Model TP-1500; Dummies Unlimited, Pomona, CA) was used in place of a live subject during scanning, while the noise measurements were acquired to replicate the patient environment. During the test, RF pulses were kept to minimums to avoid damaging the system.

The secondary acoustic wave form generator was a magnetic compatible headset with PZT (piezoelectric transducer) speakers (Resonance Technology, CA). In addition, four magnetic compatible microphones were installed. Two were located inside the headset near the

wearer's ear and measures residual acoustic response, which served as the error signal for the adaptive controller. Another two were located outside the headset and used as a reference sensor for the control system.

All other electronic equipment was located in the adjacent control room to avoid interference with the magnetic field. The ANC system developed specifically for MRI use was comprised of a dSPACE system (dSPACE GmbH, Technologiepark 25, 33100 Paderborn, Germany) running a feedforward control system developed in Matlab Simulink (The MathWorks, Inc., Natick, MA, USA). The Simulink control system was compiled on a laptop and loaded on the dSPACE processor. This processor has a high speed connection to the dSPACE input/output component, which also converts the analog signals to digital and vice versa. This hardware configuration allows for fast calculation and communication of the control signal to the headset. Since the ANC system was implemented with a digital sampling rate of 10 kHz to allow for adequate processing time, a high-speed digital recorder (Teac LX-10) was used to simultaneously record the data at 48 kHz in order to obtain the entire audible frequency range of the acoustic signals for subsequent processing. The digitized signals were then stored on the PC computer (Intel Pentium M, 1.86 GHz, 1 GB RAM) that controlled the data acquisition.

In the live scan study, three typical scanning sequences were considered for testing the performance of the developed ANC system. These three MRI scanning sequences were echo planar imaging (EPI), gradient echo multi-slice (GEMS) and Modified Driven Equilibrium Fourier Transform (MDEFT). The specific parameters used for these three scanning sequences are listed in Table 1.

Controller Design

The controller plays an important role in the ANC system. The implemented controller was a multiple reference feedforward filtered-x least mean square (FXLMS) control system. In order to preserve stability of the feedforward system, the effective frequency range was limited by the spectral characteristics of the reference signals. In our previous study, multiple reference signals were also utilized; however, the effective frequency range of the control system was limited to 2 kHz. In this experiment, a refinement was made to the previous version of the control system to extend the overall effectiveness to higher frequencies. Multiple copies of the algorithm were implemented in parallel and each one was tuned to maximize reduction of a different portion of the frequency spectrum by adding high pass frequency filters to the reference signals. Figure 1 shows the diagram of the ANC system used in this study. It utilized four different reference signals; the Z gradient (slice-selection direction in this case), the unfiltered microphone, and two different high pass filtered microphone signals. The choice of slice-selection gradient is because it yields more reduction of broadband noise components in addition to the principal harmonics in EPI when compared to other gradients according to our previous study (27). The two high pass filtered microphone reference signals were used to enhance the reduction for specific frequency ranges. The cut off frequencies of these two high pass filters were 2 kHz and 4 kHz, which correspond to the low response ranges of the secondary path as shown in Figure 5. The resulting individual algorithm control signals were combined to create the total control signal fed to the headset speakers which generated the cancellation sound. The error signals, measured by the microphones located inside the earpiece near the "patient's" ears, is the net response of the original MRI noise and the cancelling sound signal. This error signal is to be minimized by the control algorithm.

As mentioned previously, the FXLMS algorithm was used in the control system. The diagram of the typical ANC system using a standard FXLMS algorithm (28) is shown in Figure 2. The algorithm can be expressed by the following equations:

$$\mathbf{W}(n+1)=\mathbf{W}(n)-\mu\mathbf{X}'(n)e(n) \quad (1)$$

$$e(n)=d(n)+y'(n) \quad (2)$$

$$x'(n)=\hat{s}(n)*x(n)=\hat{\mathbf{s}}^T(n)\cdot\mathbf{X}(n)=\sum_{i=0}^{L-1}\hat{s}_i(n)x(n-i) \quad (3)$$

where $d(n)$ represents the original MRI response, $y'(n)$ is the cancellation sound from the control speaker, $e(n)$ is the error signals measured by the inside microphones, $x(n)$ is the reference signal (which varies for each of the algorithms in the multi-reference parallel control system), and $x'(n)$ is the filtered reference signal (*i.e.* the reference signal, $x(n)$, filtered by the secondary path model). The weighted values of the adaptive filter $W(z)$ can be expressed by vector $\mathbf{W}(n)=\begin{bmatrix} w_0(n) & w_1(n) & \cdots & w_{L-1}(n) \end{bmatrix}^T$. Vector $\mathbf{X}(n)=\begin{bmatrix} x(n) & x(n-1) & \cdots & x(n-L+1) \end{bmatrix}^T$ is formed by the current reference signal data and its previous data. Additionally, vector $\mathbf{X}'(n)$ is formed by the current filtered reference signal data and its previous data as shown here, $\mathbf{X}'(n)=\begin{bmatrix} x'(n) & x'(n-1) & \cdots & x'(n-L+1) \end{bmatrix}^T$. $\hat{s}(n)$ is the estimated impulse response of the secondary path $S(z)$, which is from the input signal for the speaker to the output signal of the error sensor. The vector $\hat{\mathbf{s}}(n)=\begin{bmatrix} \hat{s}_0(n) & \hat{s}_1(n) & \cdots & \hat{s}_{L-1}(n) \end{bmatrix}^T$ is formed by the sampled data of the impulse response of the secondary path. The parameter μ is the step size, which affects the convergence speed and stability of the algorithm.

In Situ Testing

Three typical MRI scanning sequences were tested. The baseline response (i.e. when ANC is off) for each of the three scanning sequences was recorded first. Then, the control system was tuned for the different scanning sequences by adjusting the step size of the FXLMS algorithm. Once the ANC system converged and the residual noise was constant, no further reduction was observed. Measurements at this time were made for the controlled response.

Data Processing

The recorded data was post processed and analyzed using an advanced sound data analysis software package (B&K Sound Quality) and Matlab in order to quantify and assess the performance of the proposed ANC system. Using these signal analysis software packages, the measured data was analyzed in the time and frequency domains using a variety of computational tools including SPL calculation in linear-weighted decibel (dB) and A-weighted decibel (dBA), Fourier transforms and other time-frequency processors.

RESULTS AND DISCUSSION

Time-Frequency Analysis of MRI Noise Responses

In this study, three different scanning sequences were used: GEMS, 3D MDEFT and multi-slice EPI. These three scanning sequences are commonly used in imaging and have very different signatures in both the time and frequency domains. The time histories and spectra of the noise for the three imaging protocols are shown in Figure 3(a) and (b), respectively.

The upper plots in Figures 3(a) and (b) are the recorded noises for the GEMS scanning sequence. Clearly, the MRI noise of the GEMS sequence is dominated by a cluster of harmonics in the frequency domain. In the time domain the generated noise is continuous and steady state. The middle plots are for the noise generated by the MDEFT scanning sequence. Similar to the GEMS frequency domain result, the spectrum of the MDEFT sequence is also dominated by many harmonics. Obviously, the energy distribution in the frequency domain for the MDEFT scan is different from that for the GEMS. In general, the response of higher frequency components is less than lower frequency components. Furthermore, in the time domain, the MDEFT response shows variation. One notes that there is a silent period between two segments of sound. The bottom plots are for the generated MRI noise of the EPI sequence. As seen from the results, EPI noise not only has harmonic components but also a strong broadband component. In the time domain, similar to the MDEFT result, the EPI noise exhibits varying transient behavior. A short period of silence occurs between two sound segments.

Measuring the performance of the developed ANC system on these three examples is a good evaluation of overall system performance since these three examples are commonly used for MRI scanning and cover varying acoustic signatures such as tonal and broadband noise, as well as steady state and transient sound.

Control Result of GEMS Sequence

The first test case is to control the MRI noise generated by the GEMS scanning sequence. The results are shown in Figure 4. The dotted line is the baseline response of the sound measured by the microphones inside the earpiece of headset. It illustrates that the spectrum of MRI noise during the GEMS scan is dominated by clusters of harmonics. The solid line in Figure 4 is the resulting noise measurement inside the earpiece with the ANC system operational. Compared to our previous study, the refined system extended the effective frequency range of the control system to 5 kHz, approximately 3,000 Hz higher than that of the previous system. The highest frequency harmonic exhibiting substantial reduction is above 4.5 kHz. The maximum reduction, about 55 dB, occurs at a frequency of 1.3 kHz.

There are two frequency ranges where the reduction is not significant in comparison to other harmonics. The maximum reduction for these harmonics is less than 20 dB. The first frequency range is between 2.3 kHz and 2.6 kHz. The other frequency range is above 3.9 kHz. A possible reason for less reduction occurring in these two frequency ranges is that the original response level of the harmonics within these two frequency ranges is lower than other harmonics (see more below). A second possibility may be related to the dynamics of the speaker-microphone pair, which is generally referred to as the secondary path. In fact, as shown in Figure 5, these two frequency ranges do correspond to the weak magnitude response measured for the speaker-microphone pair. For the harmonics in other frequency ranges 30 dB reduction and above are achieved.

Control result of MDEFT sequence

Unlike the GEMS sequence which generated noise continuously throughout the measurement period, the MDEFT sequence exhibits transient characteristics. There is a brief period of loud sound followed by a longer time without scanning noise. Since the length of the quiet portion exceeds the loud one, the calculated results presented are taken from a time block of data that consists of only the loud scanning period without the inclusion of the quieter interlude. The frequency domain results for this time block for the MDEFT sequence are shown in Figure 6. The dotted line is the baseline response of MRI noise and the solid line is the controlled response. Similar to the GEMS results, more reduction is obtained for the harmonics below 2 kHz. For the two frequency ranges in the GEMS test that showed less

reduction with control, no substantial reduction is achieved for the MDEFT test either. Aside from these two frequency ranges, less than 10 dB reduction is obtained for the harmonics between 3.2 kHz and 3.8 kHz. This might be due to the fact that these harmonics are much weaker in comparison to the GEMS case. The most reduction (approximately 45 dB) is observed to be at 2.7 kHz for the MDEFT test as opposed to 1.3 kHz for the GEMS test. This is because the harmonic at 1.3 kHz is not the dominant component for MDEFT. In general, less reduction is obtained for most harmonics in the MDEFT sequence when compared with the GEMS sequence. The reason may be that the MDEFT response level is lower than GEMS case.

Since the sound generated during the MDEFT scan is not continuous, it is also of interest to observe the transient results, shown in Figure 7. The upper plot, Figure 7(a), is the baseline response. The bottom plot, Figure 7(b), is the controlled response. Obviously the response level of the controlled measurement is much less than baseline measurement. Within the silent period, the controlled response is of the same level as the baseline response, which is background noise. At the beginning and end of the sound period, a brief increase can be identified in the controlled response, though it is still much lower than the baseline response. This burst may be related to the controller's characteristics changing during the relatively long silent period. Once the loud scanning noise commences, it takes a short duration for the controller to converge to the optimal solution again. In light of the fact that the MRI noise is repetitive, the optimal solution of the controller is assumed to be similar for different loud sound periods. It may be possible to set a smaller step size during the silent period to prevent the controller from shifting away from the optimal solution. This could reduce the time to re-converge to the solution when the subsequent loud period starts and consequently improve overall performance. Further study is under way to refine the system performance with this type of transient signal.

Control results of EPI sequence

The EPI sequence may be the most difficult case since it contains a strong broadband component in addition to strong harmonics. The existence of phase delay in the secondary path (control speaker to inside microphone error sensor) renders the broadband component more difficult to address. Since the noise generated by the EPI scan is not continuous, a loud time block is used for the frequency domain calculations, the same as for the MDEFT case. Similar to the previous plots, as shown in Figure 8, the dotted line represents the baseline response of EPI noise and the solid line represents the controlled response. The dominant harmonics, at about 900 Hz and 2.8 kHz, are reduced substantially. Approximately 30 dB reduction is obtained at the harmonic near 900 Hz, while more than 40 dB reduction can be seen at the harmonic around 2.8 kHz. In addition, more than 10 dB of reduction is achieved for frequencies adjacent to the 900 Hz harmonic. In our previous study (3), these frequency components were found to arise from the broadband response of EPI noise and generated by the Z-gradient excitation (slice-selection gradient).

As discussed previously, the EPI sequence exhibits a transient behavior that comprises of short silent zone followed by loud bursts repeatedly. The time history of the response before and after control for the EPI scan is shown in Figure 9. Similar to the MDEFT results, Figure 9(a) and (b) are the baseline response and the controlled response, respectively. However, the EPI sequence has a much shorter silent period in comparison to the MDEFT. There is also no increase in the controlled response at the beginning and end of the sound period as was observed during the MDEFT scan. This may be a result of the silent period being short enough to prevent a change in the characteristics of the controller dramatically. The controller is still nearly optimal when the next loud period begins.

Summary of Three Cases

In this study, we developed an active headset system and tested the performance *in situ*. Experimental work was conducted on three common MRI scanning sequences, namely GEMS, MDEFT and EPI. Substantial reduction in noise levels at the patient's ear was obtained in each of the tests. The greatest reduction, about 55 dB, was achieved at the harmonic at a frequency of 1.3 kHz in the GEMS case. Approximately 21 dB and 30 dBA overall reduction was achieved for GEMS noise across the entire audible frequency range. For the MDEFT sequence, the control system achieved 14 dB and 14 dBA overall reduction over the audible frequency range, while 13 dB and 14 dBA reduction was obtained for the EPI case. These linear-weighted and A-weighted SPLs are calculated using the B&K Sound Quality software package. Only the time blocks representing the loud sound periods for the MDEFT and EPI cases were used in the calculation of frequency domain response and SPLs. Also, note that these results represent the reduction due to the active control only. Since the measurements were obtained inside the earpiece, the contribution of passive reduction of the headset has already taken place for all tests, with and without the controller active. The total noise reduction a patient would observe compared to the ambient level during scanning would be a combination of the headset passive reduction and the active control reduction. By comparing the outside and inside microphone responses, the passive reduction attributed to the headset can be evaluated. For GEMS noise, about 16 dB and 20 dBA reduction can be obtained by passive means. The MDEFT scan produced 15 dB and 19 dBA reduction. In the final scanning sequence, EPI, 18 dB and 18 dBA reduction were measured. Note that all passive reductions reported in this study appear to be less than prior work. This is because the acoustic noise reduction for each scanning sequence tested was assessed over the entire audible frequency range. In fact, the passive reduction of our headset is about 30 dB for frequencies higher than 1 kHz, which is very similar to the test results shown by Ravicz, et al (11). The detailed measured attenuation for these three scanning sequences by active and passive means are summarized in the Table 2. Since the proposed ANC system uses adaptive algorithm, the system is designed to adapt as the MRI noise varies due to the change of scanning parameters such as the number of the slices or the TR.

In conclusion, the proposed ANC system works well on noise generated during a variety of common MRI scanning sequences. *In situ* testing was conducted during live scans on a 4 T MRI for three scanning sequences, namely GEMS, MDEFT and EPI. Very promising results were obtained. These results demonstrated potential for the development of a commercial product that could provide a substantial level of noise reduction for the patient. Up to this point, the results reported herehave been objective measurements. Future work should consider subjective feedback from human subjects. It may be possible that the perceived performance of the control system is less effective than objective evaluation due to other paths (e.g. bone conduction). However, the impact is expected to be small due to the high impedance mismatch between the surrounding air and the skull structure (29, 30). The ANC system is headset based, therefore, it is relatively easy to implement onto any existing MRI system..

Acknowledgments

Grant Support:

This paper is supported by the National Institute of Biomedical Imaging and Bioengineering (EB005042) and the National Institute for Occupational Safety and Health (NIOSH) University of Cincinnati Education and Research Center grant (T42/OH008432-05)

We thank Mr. Jeffrey Osterhage from the Center for Imaging Research for providing technical support in setting up the MRI experiments for this study. We also acknowledge Resonance Technology, Inc., for supplying the headphones utilized in this study.

References

1. Hurwitz R, Lane S, Bell RA, Zawadzki MN. Acoustic analysis of gradient coil noise in MR imaging. Radiology. 1989; 173:545–548. [PubMed: 2798888]
2. Ravicz ME, Melcher JR, Kiang NY. Acoustic noise during functional magnetic resonance imaging. J Acoust Soc Am. 2000; 108 :1683–1696. [PubMed: 11051496]
3. More SR, Lim TC, Li M, Holland CK, Boyce SE, Lee J-H. Acoustic noise characteristics of a 4 Tesla MRI scanner. J Magn Reson Imaging. 2006; 23:388–397. [PubMed: 16463341]
4. Gangarosa RE, Minnis JE, Nobbe J, Praschan D, Genberg RW. Operational safety issues in MRI. Magn Reson Imaging. 1987; 5 :287–92. [PubMed: 3657401]
5. Quirk ME, Letendre A, Ciottone RA, Lingley JF. Anxiety in patients undergoing imaging. Radiology. 1989; 170:463–466. [PubMed: 2911670]
6. McJury M, Shellock F. Auditory noise associated with MR procedures: A review. J Magn Reson Imaging. 2000; 12:37–45. [PubMed: 10931563]
7. Brummett RE, Talbot JM, Charubas P. Potential hearing loss resulting from MR imaging. Radiology. 1988; 169:539–540. [PubMed: 3175004]
8. Counter SA, Bjelke B, Klason T, Chen Z, Borg E. Magnetic resonance imaging of the cochlea, spiral ganglia and eighth nerve of the guinea pig. Neuroreport. 1999; 10:473–479. [PubMed: 10208574]
9. Foster JR, Hall DA, Summerfield AQ, Palmer AR, Bowtell RW. Sound-level measurements and calculations of safe noise dosage during EPI at 3 T. J Magn Reson Imaging. 2000; 12:157–163. [PubMed: 10931575]
10. Shellock FG, Ziarati M, Atkinson D, Chen DY. Determination of gradient magnetic field-induced acoustic noise associated with the use of echo planar and three-dimensional, fast spin echo techniques. J Magn Reson Imaging. 1998; 8:1154–1157. [PubMed: 9786155]
11. Ravicz ME, Melcher JR. Isolating the auditory system from acoustic noise during functional magnetic resonance imaging: examination of noise conduction through the ear canal, head, and body. J Acoust Soc Am. 2001; 109 :216–231. [PubMed: 11206150]
12. Mansfield P, Glover PM, Beaumont J. Sound generation in gradient coil structures for MRI. Magn Reson Med. 1998; 39:539–550. [PubMed: 9543415]
13. Hedeen RA, Edelstein WA. Characterization and prediction of gradient acoustic noise in MR imagers. Magn Reson Med. 1997; 37:7–10. [PubMed: 8978626]
14. Lee JH, Rudd B, Li M, Lim TC. Sound reduction technologies for MRI scanners. Recent Patents on Engineering. 2008; 2:72–79.
15. Hennel F, Girard F, Loenneker T. “Silent” MRI with soft gradient pulses. Magn Reson Med. 1999; 42:6–10. [PubMed: 10398943]
16. Goldman AM, Gossman WE, Friedlander PC. Reduction of sound levels with antinoise in MR imaging. Radiology. 1989; 173:549–550. [PubMed: 2798889]
17. Pla, FG.; Sommerfeldt, SD.; Hedeen, RA. Active control of noise in magnetic resonance imaging. Proceeding of Active 95; Newport Beach, CA, USA. 1995. p. 573-582.
18. Mcjury M, Stewart RW, Crawford D, Toma E. The use of active noise control (ANC) to reduce acoustic noise generated during MRI scanning: some initial results. Magn Reson Imaging. 1997; 15:319–322. [PubMed: 9201679]
19. Chen CK, Chiueh TD, Chen JH. Active cancellation system of acoustic noise in MR imaging. IEEE Trans Biomed Eng. 1999; 46:186–191. [PubMed: 9932340]
20. Mechefske CK, Geris R, Gati JS, Rutt BK. Acoustic Noise Reduction in a 4T MRI Scanner. MAGMA. 2002; 13:172–6. [PubMed: 11755093]
21. Kahana, Y.; Alexander, Kots; Mican, S.; Chambers, J.; Bullock, D. Optoacoustical ear defenders with active noise reduction in an MRI communication systems. Proceeding of Active 04; Virginia, USA: Williamsburg; 2004. paper a04_067

22. Chambers J, Akeroyd MA, Summerfield AQ, Palmer AR. Active control of the volume acquisition noise in functional magnetic resonance imaging: method and psychoacoustical evaluation. J Acoust Soc Am. 2001; 110:3041–3054. [PubMed: 11785805]

23. Chambers J, Bullock D, Kahana Y, Kots A, Palmer A. Developments in active noise control sound systems for magnetic resonance imaging. Applied Acoustic. 2007; 68:281–295.

24. Hall DA, Chambers J, Akeroyd MA, Foster JR, Coxon R, Palmer AR. Acoustic, psychophysical, and neuroimaging measurements of the effectiveness of active cancellation during auditory functional magnetic resonance imaging. J Acoust Soc Am. 2009; 125:347–359. [PubMed: 19173422]

25. Li M, Lim TC, Lee J-H. Simulated study on active noise control for a 4-T MRI scanner. Magn Reson Imaging. 2008; 26:393–400. [PubMed: 18060719]

26. Rudd, BW.; Lim, TC.; Li, M.; Lee, J-H. Feedforward active noise cancellation for MRI utilizing reference microphone. Proceedings of Active 2009; Ottawa, Ontario, Canada. 2009. Paper No. ac09-968

27. Rudd, BW.; Lim, TC.; Li, M.; Lee, J-H. In-situ active noise cancellation applied to magnetic resonance imaging. Proceedings of IMECE 2009; Lake Buena Vista, Florida, USA . 2009. Paper No. IMECE2009-11337

28. Kuo, SM.; Morgan, DR. Active noise control systems: algorithms and DSP implementations. New York: John Wiley & Sons, Inc; 1996.

29. Kinsler, LE.; Frey, AR.; Coppens, AB.; Sanders, JV. Fundamentals of Acoustics. John Wiley & Sons, Inc; 2000.

30. Katz BFG. Acoustic absorption measurement of human hair and skin within audible frequency range. J Acoust Soc Am. 2000; 108:2238–2242. [PubMed: 11108363]

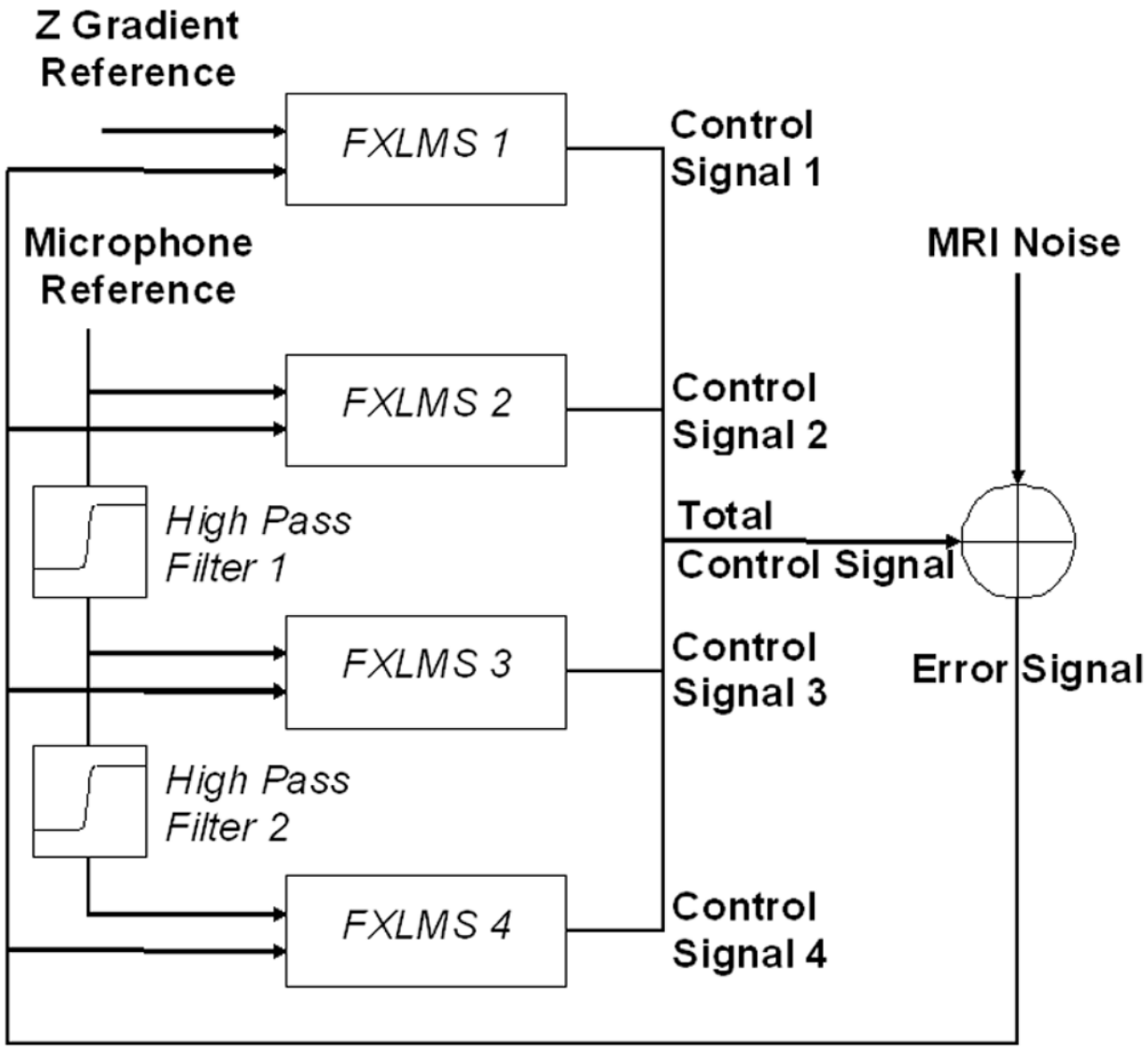

Figure 1.
Refined multiple reference FXLMS algorithm used in the control system.

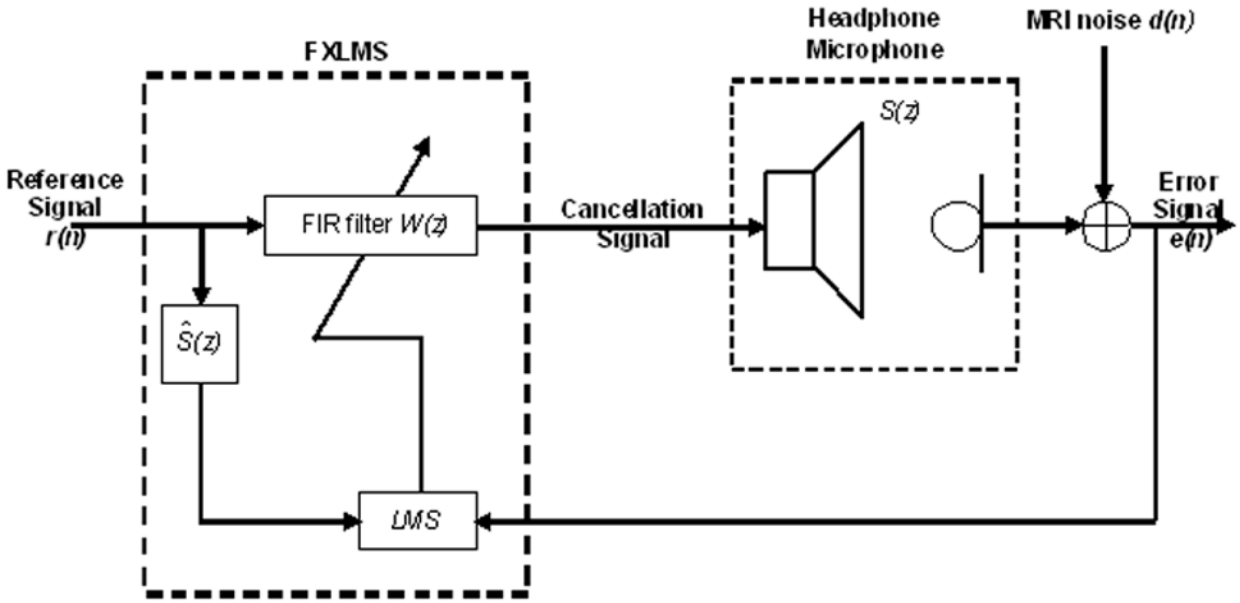

Figure 2.
Diagram of active control system with standard FXLMS algorithm.

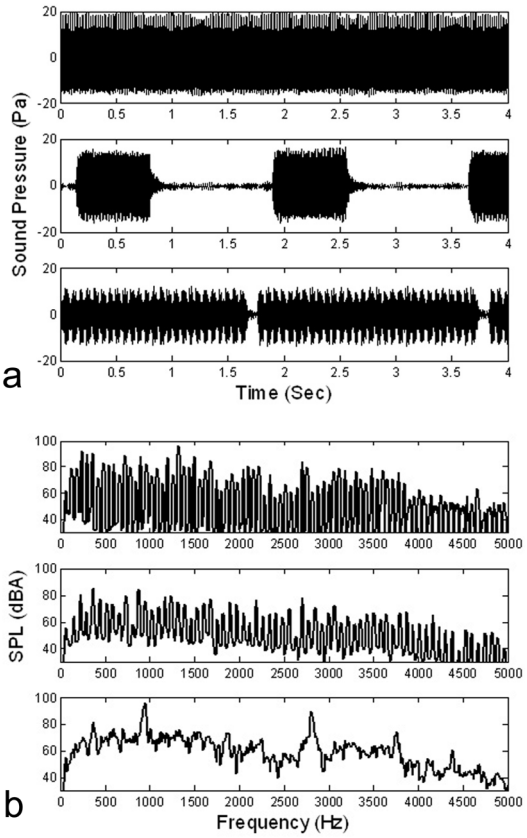

Figure 3.
Time histories and spectra of baseline responses of the MRI noise for three tested scanning sequences (GEMS, MDEFT, and EPI, from top to bottom).

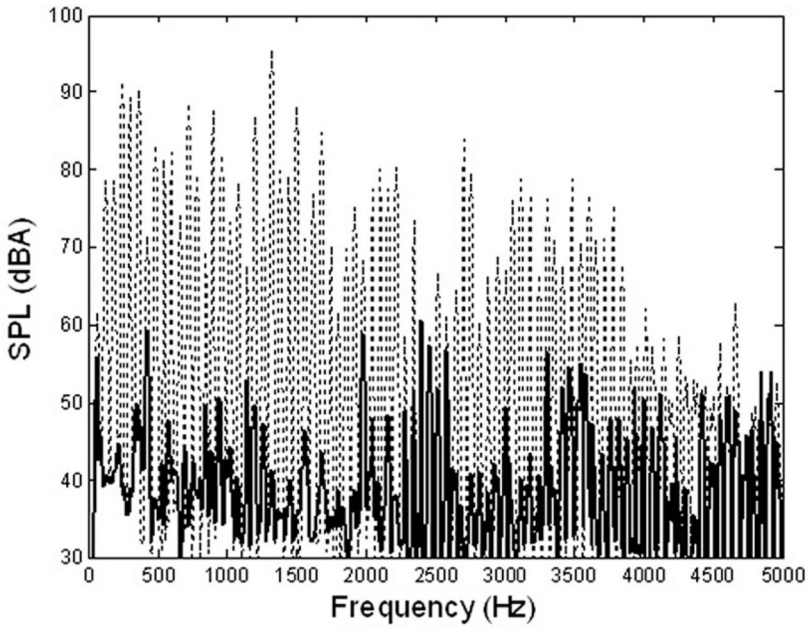

Figure 4.

In situ control results of GEMS scanning sequence in frequency domain (·····: baseline response; ——: controlled response).

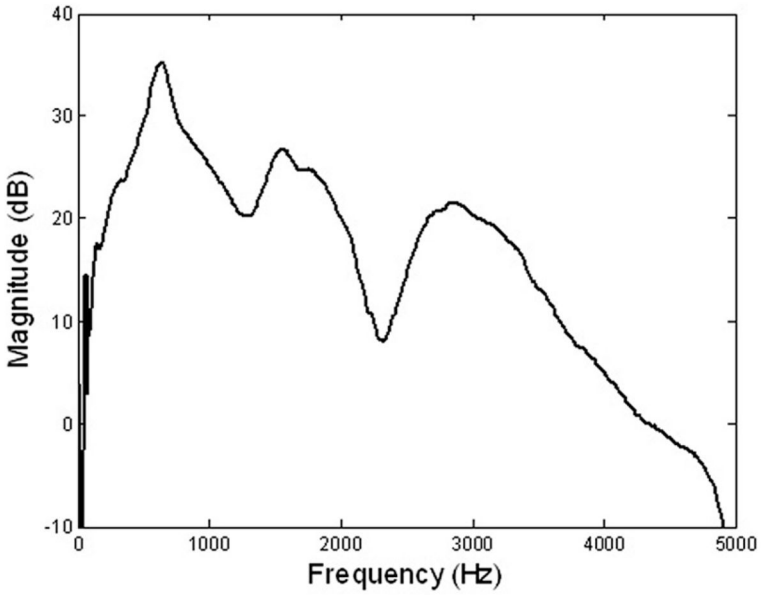

Figure 5.
Measured dynamic response of speaker-microphone pair.

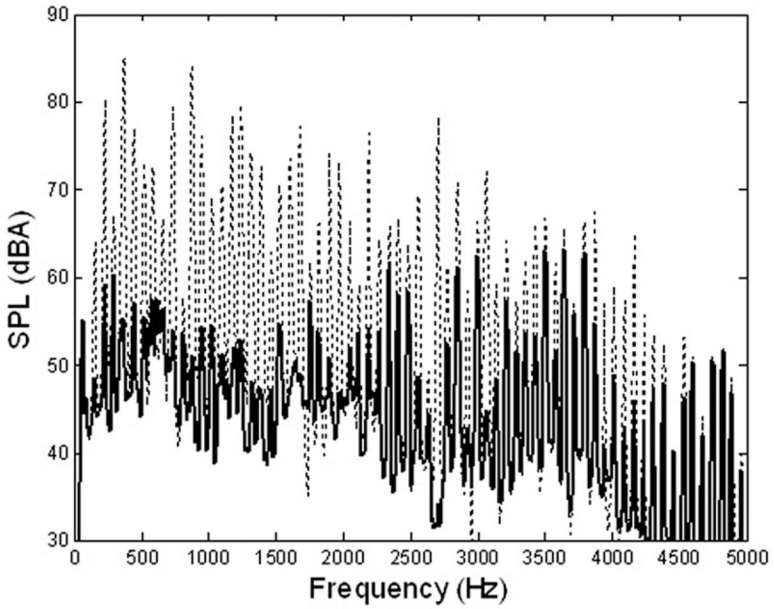

Figure 6.

In situ control results of MDEFT scanning sequence in frequency domain (·····: baseline response; ——: controlled response).

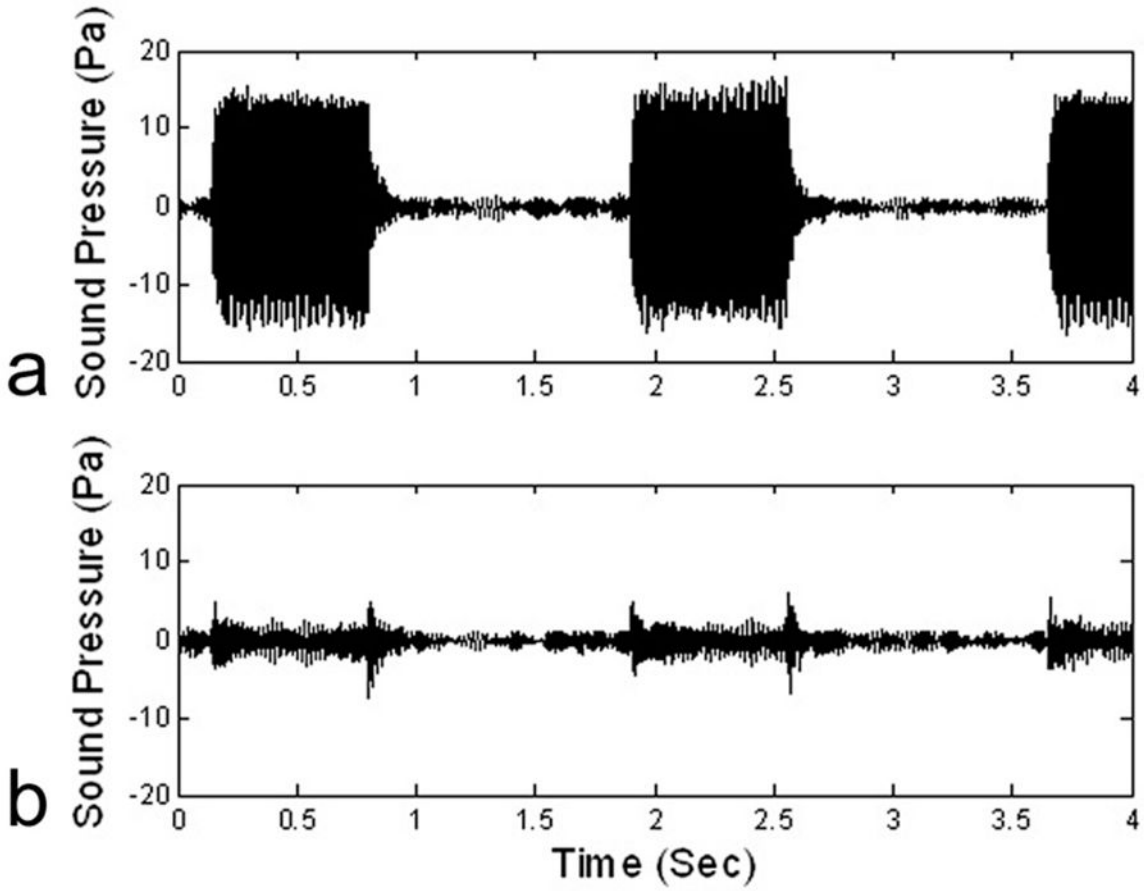

Figure 7.
In situ control results of MDEFT scanning sequence in time domain (a : baseline response; b: controlled response).

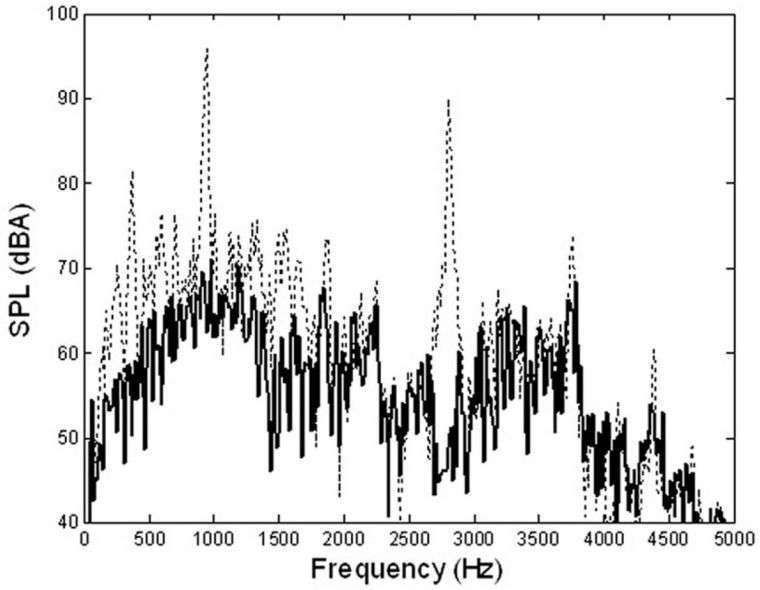

Figure 8.

In situ control results of EPI scanning sequence in frequency domain (·····: baseline response; ———: controlled response).

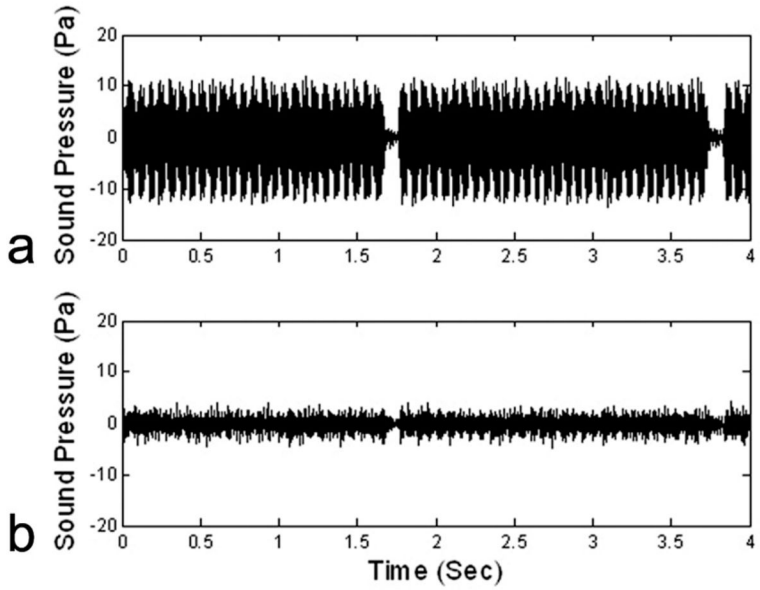

Figure 9.
In situ control results of EPI scanning sequence in time domain (a: baseline response; b: controlled response).

Table 1

MRI scanning sequences' parameters employed in the experiments.

Sequence	Time Interval (TR) (ms)	Echo Time (TE) (ms)	Bandwidth (BW) (kHz)
GEMS	10	5	100000
MDEFT	15	6	100000
EPI	2000	30	125000

Table 2

Measured attenuations over the entire audible frequency range by active and passive means for three different sequences.

Sequence	Active Means		Passive Means		Total	
	dB	dBA	dB	dBA	dB	dBA
GEMS	21	30	16	20	37	50
MDEFT	14	14	15	19	29	33
EPI	13	14	18	18	31	32